A global function of climatic aridity accounts for soil moisture stress on carbon assimilation

Giulia Mengoli[1], Sandy P. Harrison[2,3], I. Colin Prentice[1,3]

1: Georgina Mace Centre for the Living Planet, Department of Life Sciences, Imperial College London, Silwood Park Campus, Buckhurst Road, Ascot, SL5 7PY, UK

2: Department of Geography and Environmental Science, School of Archaeology, Geography and Environmental Science (SAGES), University of Reading, Reading, RG6 6AH, UK

3: Ministry of Education Key Laboratory for Earth System Modelling, Department of Earth System Science, Tsinghua University, Beijing 100084, China

Correspondence to: Giulia Mengoli (gmengoli@ic.ac.uk)

Supplementary Information

This Supplementary Information contains the following tables and figures:

Supplementary Table 1. Characteristics of the flux tower sites used in the analysis, giving the unique code for each site (Site ID), latitude, longitude, elevation, calculated aridity index (AI), climate classification, vegetation classification, sampling years (recording period) and reference. The climate type follows Köppen system, where Aw is tropical savanna, Am is tropical monsoon, BSk is cold semi-arid or steppe, BSh is hot semi-arid or steppe, BWh is hot arid desert, Csa is temperate with dry hot summer, Cfa is temperate with no dry season and hot summer, Cfb is temperate with no dry season and warm summer, Cwa is temperate with dry winter and hot summer, Dfc is continental with no dry season and cold summer, Dwb is continental with dry winter and warm summer, Dfb is continental with no dry season and warm summer, and ET is polar tundra. The ecosystem type is based on the International Geosphere–Biosphere Programme (IGBP) definition, where ENF is evergreen needleaf forest, DBF is deciduous broadleaf forest, EBF is evergreen broadleaf forest, MF is mixed forest, WSA is woody savanna, SAV is savanna, CSH is closed shrubland, OSH is open shrubland, and GRA is grassland.

Supplementary Figure 1: Box-plot showing the range of intercept values obtained across all the flux tower sites, grouped by aridity class. The black line is the median value, the box is the interquartile range and the whiskers show the range, with outliers shown as asterisks. The median value is not significantly different from zero.

Supplementary Figure 2: Values of the fitted maximum $\beta(\theta)$ ratio (the ratio of actual flux-derived to modelled well-watered gross primary production) and the critical threshold value of soil moisture for all 67 sites used in the analysis, where the intercept is assumed to be zero. The $\beta(\theta)$ ratio and the soil water content (swc) are both unitless. Note that the scale above 1 has been compressed for visualization purposes.

Supplementary Figure 3: Values of the fitted maximum $\beta(\theta)$ ratio (the ratio of actual flux-derived to modelled well-watered gross primary production) and the critical threshold value of soil moisture for all 67 sites used in the analysis, where the intercept is assumed to be zero (green line) or not fixed (red line). The $\beta(\theta)$ ratio and the soil water content (swc) are both unitless. Note that the scale above 1 has been compressed for visualization purposes.

Supplementary Figure 4: The fitted non-linear regression model of the maximum level (top) and the critical threshold (bottom) of the $\beta(\theta)$ ratio (the ratio of observed to predicted gross primary production) against the aridity index, where the sites are classified according to vegetation type and precipitation phase.

Supplementary Figure 5: The fitted non-linear regression model of the maximum level (top) and the critical threshold (bottom) of the $\beta(\theta)$ ratio (the ratio of observed to predicted gross primary production) against the aridity index, where the sites are classified according to vegetation type and precipitation concentration.

Supplementary Figure 6: The impact of the application of the new soil moisture stress function on simulated gross primary production (GPP_{new}) at flux tower sites classified as arid (aridity index, AI >5). The new model is compared to the simulated level of GPP under well-watered conditions (GPP_{ww}) and to flux-derived values (GPP_{obs}).

Supplementary Figure 7: The impact of the application of the new soil moisture stress function on simulated gross primary production (GPP_{new}) at flux tower sites classified as semi-arid (aridity index, AI between 2 and 5). The new model is compared to the simulated level of GPP under well-watered conditions (GPP_{ww}) and to flux-derived values (GPP_{obs}).

Supplementary Figure 8: The impact of the application of the new soil moisture stress function on simulated gross primary production (GPP_{new}) at flux tower sites classified as humid (aridity index, AI <2). The new model is compared to the simulated level of GPP under well-watered conditions (GPP_{ww}) and to flux-derived values (GPP_{obs}).

Supplementary Figure 9: Comparison of simulated gross primary production including the new soil-moisture stress function (GPP_{new}) and the original stress function ($GPP_{v1.0}$) from Stocker et al. (2020) against flux-derived values (GPP_{obs}) at flux tower sites classified as arid (aridity index, AI > 5).

Supplementary Figure 10: Comparison of simulated gross primary production including the new soil-moisture stress function (GPP_{new}) and the original stress function ($GPP_{v1.0}$) from Stocker et al. (2020) against flux-derived values (GPP_{obs}) at flux tower sites classified as semi-arid (aridity index, AI = between 2 and 5).

Supplementary Figure 11: Comparison of simulated gross primary production including the new soil-moisture stress function (GPP_{new}) and the original stress function ($GPP_{v1.0}$) from Stocker et al. (2020) against flux-derived values (GPP_{obs}) at flux tower sites classified as humid (aridity index, AI < 2).

Supplementary Table 1. Characteristics of the flux tower sites used in the analysis, giving the unique code for each site (Site ID), latitude, longitude, elevation, calculated aridity index (AI), climate classification, vegetation classification, sampling years (recording period) and reference. The climate type follows Köppen system, where Aw is tropical savanna, Am is tropical monsoon, BSk is cold semi-arid or steppe, BSh is hot semi-arid or steppe, BWh is hot arid desert, Csa is temperate with dry hot summer, Cfa is temperate with no dry season and hot summer, Cfb is temperate with no dry season and warm summer, Cwa is temperate with dry winter and hot summer, Dfc is continental with no dry season and cold summer, Dwb is continental with dry winter and warm summer, Dfb is continental with no dry season and warm summer, and ET is polar tundra. The ecosystem type is based on the International Geosphere–Biosphere Programme (IGBP) definition, where ENF is evergreen needleaf forest, DBF is deciduous broadleaf forest, EBF is evergreen broadleaf forest, MF is mixed forest, WSA is woody savanna, SAV is savanna, CSH is closed shrubland, OSH is open shrubland, and GRA is grassland.

Site ID	Latitude (°)	Longitude (°)	Elevation (m)	AI	Climate	IGBP	Recording period	Reference
AR-SLu	-33.46	-66.46	507	2.89	BSk	MF	2009-2011	Ulke et al. (2015)
AR-Vir	-28.24	-56.19	104	1.02	Cfa	ENF	2009-2012	Posse et al. (2016)
AU-Ade	-13.08	131.12	79	1.55	Aw	WSA	2007-2009	Beringer et al. (2011b)
AU-ASM	-22.28	133.25	605	6.97	BSh	SAV	2010-2013	Cleverly et al. (2013)
AU-Cpr	-34.00	140.59	60	6.36	BSk	SAV	2010-2014	Meyer et al. (2015)
AU-DaP	-14.06	131.32	69	1.80	Aw	GRA	2007-2013	Beringer et al. (2011a)
AU-DaS	-14.16	131.39	79	1.81	Aw	SAV	2010-2014	Hutley et al. (2011)
AU-Dry	-15.26	132.37	175	2.32	Aw	SAV	2008-2014	Cernusak et al. (2011)
AU-Emr	-23.86	148.47	175	3.08	BSh	GRA	2011-2013	Schroder et al. (2014)
AU-Gin	-31.38	115.71	50	2.93	Csa	WSA	2012-2014	Beringer et al. (2016)
AU-GWW	-30.19	120.65	446	5.75	BSh	SAV	2013-2014	Prober et al. (2012)
AU-How	-12.49	131.15	35	1.46	Aw	WSA	2003-2008	Beringer et al. (2007)
AU-Lox	-34.47	140.66	43	6.32	BSk	DBF	2008-2009	Stevens et al. (2011)
AU-RDF	-14.56	132.48	181	2.16	Aw	WSA	2011-2013	Bristow et al. (2016)
AU-Rig	-36.65	145.58	151	1.81	Cfb	GRA	2011-2014	Beringer et al. (2016)
AU-Stp	-17.15	133.35	229	3.71	BSh	GRA	2010-2014	Beringer et al. (2011a)
AU-TTE	-22.29	133.64	551	7.17	BWh	GRA	2012-2013	Cleverly et al. (2016)
AU-Tum	-35.66	148.15	1238	1.34	Cfb	EBF	2007-2014	Leuning et al. (2005)
AU-Wac	-37.43	145.19	732	1.69	Cfb	EBF	2005-2008	Kilinc et al. (2013)
AU-Whr	-36.67	145.03	144	2.39	Cfb	EBF	2011-2014	McHugh et al. (2017)
AU-Wom	-37.42	144.09	700	1.75	Cfb	EBF	2010-2012	Hinko-Najera et al. (2017)
AU-Ync	-34.99	146.29	127	3.96	BSk	GRA	2012-2014	Yee et al. (2015)
BE-Bra	51.31	4.52	16	0.91	Cfb	MF	2007-2014	Carrara et al. (2004)
BE-Vie	50.30	6.00	486	0.73	Cfb	MF	2010-2014	Aubinet et al. (2001)
BR-Sa3	-3.02	-54.97	172	0.78	Am	EBF	2001-2004	Wick et al. (2005)
CA-Man	55.88	-98.48	261	1.19	Dfc	ENF	2003-2008	Dunn et al. (2007)
CA-NS4	55.91	-98.38	252	1.19	Dfc	ENF	2002-2005	Chu et al. (2021)
CA-SF3	54.09	-106.01	544	1.41	Dfc	OSH	2002-2006	Chu et al. (2021)
CH-Fru	47.12	8.54	972	0.71	Cfb	GRA	2007-2014	Imer et al. (2013)
CH-Oe1	47.29	7.73	454	0.80	Cfb	GRA	2003-2008	Ammann et al. (2009)
CN-Du2	42.05	116.28	1321	2.70	Dwb	GRA	2006-2008	Chen et al. (2009)
CN-HaM	37.37	101.18	4032	2.34	ET	GRA	2002-2004	Kato et al. (2006)
CZ-BK2	49.49	18.54	844	0.78	Dfb	GRA	2004-2006	NA

DE-Gri	50.95	13.51	380	1.18	Cfb	GRA	2010-2014	Prescher et al. (2010)
DE-RuR	50.62	6.30	514	0.78	Cfb	GRA	2011-2014	Post et al. (2015)
ES-LgS	37.10	-2.97	2271	2.88	Csa	OSH	2007-2009	Reverter et al. (2010)
ES-Ln2	36.97	-3.48	2215	3.84	Csa	OSH	2009-2009	Serrano-Ortiz et al. (2011)
FI-Hyy	61.85	24.29	177	0.87	Dfc	ENF	2010-2014	Suni et al. (2003)
FR-Fon	48.48	2.78	93	1.39	Cfb	DBF	2007-2013	Delpierre et al. (2015)
FR-LBr	44.72	-0.77	63	1.10	Cfb	ENF	2003-2008	Berbigier et al. (2001)
FR-Pue	43.74	3.60	269	1.57	Csa	EBF	2003-2007	Rambal et al. (2004)
IT-Col	41.85	13.59	1549	1.35	Cfa	DBF	2007-2014	Valentini et al. (1996)
IT-Cp2	41.70	12.36	3	1.73	Csa	EBF	2012-2014	Fares et al. (2014)
IT-MBo	46.01	11.05	1549	1.18	Dfb	GRA	2007-2013	Marcolla et al. (2011)
IT-Noe	40.61	8.15	29	2.26	Csa	CSH	2004-2008	Papale et al. (2014)
IT-SRo	43.73	10.28	3	1.34	Csa	ENF	2003-2008	Chiesi et al. (2005)
IT-Tor	45.84	7.58	2164	0.63	Dfc	GRA	2008-2014	Galvagno et al. (2013)
NL-Hor	52.24	5.07	1	0.84	Cfb	GRA	2006-2011	Jacobs et al. (2007)
RU-Fyo	56.46	32.92	268	0.97	Dfb	ENF	2010-2014	Kurbatova et al. (2008)
RU-Ha1	54.73	90.00	453	1.11	Dfc	GRA	2002-2004	Marchesini et al. (2007)
US-AR1	36.43	-99.42	612	2.49	Cfa	GRA	2009-2012	Chu et al. (2021)
US-AR2	36.64	-99.60	645	2.61	BSk	GRA	2009-2012	Chu et al. (2021)
US-ARb	35.55	-98.04	423	2.04	Cfa	GRA	2005-2006	Fischer et al. (2012)
US-ARc	35.55	-98.04	423	2.04	Cfa	GRA	2005-2006	Fischer et al. (2012)
US-Cop	38.09	-109.39	1903	3.99	BSk	GRA	2002-2007	Bowling et al. (2010)
US-KS2	28.61	-80.67	2	1.21	Cfa	CSH	2003-2006	Powell et al. (2006)
US-PFa	45.95	-90.27	471	1.02	Dfb	MF	2010-2014	Desai et al. (2015)
US-SRG	31.79	-110.83	1293	5.08	BSk	GRA	2008-2014	Scott et al. (2015a)
US-SRM	31.82	-110.87	1113	5.02	BSk	WSA	2008-2014	Scott et al. (2009)
US-Syv	46.24	-89.35	544	1.01	Dfb	MF	2010-2014	Desai et al. (2005)
US-Ton	38.43	-120.97	174	2.23	Csa	WSA	2003-2007	Baldocchi et al. (2010)
US-Var	38.41	-120.95	166	2.22	Csa	GRA	2008-2014	Ma et al. (2007)
US-Whs	31.74	-110.05	1372	5.89	BSk	OSH	2007-2014	Scott et al. (2015a)
US-Wi6	46.62	-91.30	354	1.08	Dfb	OSH	2002-2003	Noormets et al. (2007)
US-Wkg	31.74	-109.94	1515	6.34	BSk	GRA	2007-2014	Scott et al. (2010)
ZA-Kru	-25.02	31.50	357	2.69	Cwa	SAV	2005-2010	Archibald et al. (2009)
ZM-Mon	-15.44	23.25	1087	2.18	Aw	DBF	2003-2008	Merbold et al. (2009)

References for Table 1

Ammann, C., Spirig, C., Leifeld, J., and Neftel, A.: Assessment of the nitrogen and carbon budget of two managed temperate grassland fields, Agric. Ecosyst. Environ., 133, 150–162, 2009.

Archibald, S.A., Kirton, A., van der Merwe, M.R., Scholes, R.J., Williams, C.A., and Hanan, N.: Drivers of inter-annual variability in Net Ecosystem Exchange in a semi-arid savanna ecosystem, South Africa, Biogeosci., 6, 251–266, 2009.

Aubinet, M., Chermanne, B., Vandenhaute, M., Longdoz, B., Yernaux, M., and Laitat, E.: Long term carbon dioxide exchange above a mixed forest in the Belgian Ardennes, Agric. For. Meteorol., 108, 293–315, 2001.

Baldocchi, D., Chen, Q., Chen, X., Ma, S., Miller, G., Ryu, Y., Xiao, J., Wenk, R., Battles, J.: The dynamics of energy, water, and carbon fluxes in a blue oak (*Quercus douglasii*) savanna in California, Ecosyst. Funct. Savannas, 132, 135-151, 2010

Berbigier, P., Bonnefond, J.-M. and Mellmann, P.: CO_2 and water vapour fluxes for 2 years above Euroflux forest site, Agric. For. Meteorol., 108, 183–197, 2001.
Beringer, J., Hutley, L.B., Tapper, N.J., and Cernusak, L.A.: Savanna fires and their impact on net ecosystem productivity in North Australia, Glob. Chang. Biol., 13, 990–1004, 2007.
Beringer, J., Hutley, L.B., Hacker, J.M., Neininger, B., and Tha Paw U.K.: Patterns and processes of carbon, water and energy cycles across northern Australian landscapes: From point to region, Agric. For. Meteorol., 151, 1409–1416, 2011a.
Beringer, J., Hacker, J., Hutley, L.B., Leuning, R., Arndt, S.K., Amiri, R., Bannehr, L., Cernusak, L., Grover, S., Hensley, C., Hocking, D., Isaac, P., Jamali, H., Kanniah, K., Livesley, S., Neininger, B., Tha Paw U.K., Sea, W., Straten, D., Tapper, N., Weinmann, R., Wood, S., and Zegelin, S.: SPECIAL—Savanna patterns of energy and carbon integrated across the landscape, Bull. Am. Meteorol. Soc., 92, 1467–1485, 2011b.
Beringer, J., Hutley, L.B., McHugh, I., Arndt, S.K., Campbell, D., Cleugh, H.A., Cleverly, J., Resco de Dios, V., Eamus, D., Evans, B., Ewenz, C., Grace, P., Griebel, A., Haverd, V., Hinko-Najera, N., Huete, A., Isaac, P., Kanniah, K., Leuning, R., Liddell, M.J., Macfarlane, C., Meyer, W., Moore, C., Pendall, E., Phillips, A., Phillips, R.L., Prober, S.M., Restrepo-Coupe, N., Rutledge, S., Schroder, I., Silberstein, R., Southall, P., Yee, M.S., Tapper, N.J., van Gorsel, E., Vote, C., Walker, J., and Wardlaw, T.: An introduction to the Australian and New Zealand flux tower network – OzFlux, Biogeosci., 13, 5895–5916, https://doi.org/10.5194/bg-13-5895-2016, 2016.
Bowling, D.R., Bethers-Marchetti, S., Lunch, C.K., Grote, E.E., and Belnap. J.: Carbon, water, and energy fluxes in a semiarid cold desert grassland during and following multiyear drought, J. Geophys. Res., 115, G04026, doi:10.1029/2010JG001322, 2010.
Bristow, M., Hutley, L.B., Beringer, J., Livesley, S.J., Edwards, A.C., and Arndt, S. K.: Quantifying the relative importance of greenhouse gas emissions from current and future savanna land use change across northern Australia, Biogeosci., 13, 6285–6303, 2016.
Carrara, A., Janssens, I.A., Curiel Yuste, J., and Ceulemans, R.: Seasonal changes in photosynthesis, respiration and NEE of a mixed temperate forest, Agric. For. Meteorol., 126, 15–31, 2004.
Cernusak, L. A., Hutley, L.B., Beringer, J., Holtum, J.A.M. and Turner, B.L.: Photosynthetic physiology of eucalypts along a sub-continental rainfall gradient in northern Australia, Agric. For. Meteorol., 151, 1462–1470, 2011.
Chen, S., Chen, J., Lin, G., Zhang, W., Miao, H., Wei, L., Huang, J., and Han, X.: Energy balance and partition in Inner Mongolia steppe ecosystems with different land use types, Agric. For. Meteorol., 149, 1800–1809, 2009.
Chiesi, M., Maselli, F., Bindi, M., Fibbi, L., Cherubini, P., Arlotta, E., Tirone, G., Matteucci, G., and Seufert, G.: Modelling carbon budget of Mediterranean forests using ground and remote sensing measurements, Agric. For. Meteorol., 135, 22–34, 2005.
Chu, H., Luo, X., Ouyang, Z., Chan, W.S., Dengel, S., Biraud, S.C., Torn, M.S., Metzger, S., Kumar, J., Arain, M.A., Arkebauer, T.J., Baldocchi, D., Bernacchi, C., Billesbach, D., Black, T.A., Blanken, P.D., Bohrer, G., Bracho, R., Brown, S., Brunsell, N.A., Chen, J., Chen, X., Clark, K., Desai, A.R., Duman, T., Durden, D., Fares, S., Forbrich, I., Gamon, J. A., Gough, C.M., Griffis, T., Helbig, M., Hollinger, D., Humphreys, E., Ikawa, H., Iwata, H., Ju, Y., Knowles, J.F., Knox, S.H., Kobayashi, H., Kolb, T., Law, B., Lee, X., Litvak, M., Liu, H., Munger, J.W., Noormets, A., Novick, K., Oberbauer, S.F., Oechel, W., Oikawa, P., Papuga, S.A., Pendall, E., Prajapati, P., Prueger, J., Quinton, W.L., Richardson, A.D., Russell, E.S., Scott, R.L., Starr, G., Staebler, R., Stoy, P.C., Stuart-Haëntjens, E., Sonnentag, O., Sullivan, R.C., Suyker, A., Ueyama, M., Vargas, R., Wood, J.D., and Zona, D.: Representativeness of eddy-covariance flux footprints for areas surrounding Ameriflux sites, Agric. For. Met., 301-30, 108350, doi.org/10.1016/J.AGRFORMET.2021.108350, 2021.
Cleverly, J., Boulain, N., Villalobos-Vega, R., Grant, N., Faux, R., Wood, C., Cook, P.G., Yu, Q., Leigh, A., and Eamus, D.: Dynamics of component carbon fluxes in a semi-arid Acacia woodland, central Australia, J. Geophys. Res. Biogeosci., 118, 1168–1185, 2013.

Cleverly, J., Eamus, D., Restrepo Coupe, N., Chen, C., Maes, W., Li, L., Faux, R., Santini, N.S., Rumman, R., Yu, Q., and Huete, A.: Soil moisture controls on phenology and productivity in a semi-arid critical zone, Sci. Total Envir., 568, 1227-1237, doi: 10.1016/j.scittotenv.2016.05.14, 2016.

Delpierre, N., Berveiller, D., Granda, E., and Dufrêne, E.: Wood phenology, not carbon input, controls the interannual variability of wood growth in a temperate oak forest, New Phytol., 210, 459–470, 2016.

Desai, A.R., Bolstad, P.V., Cook, B.D., Davis, K.J., and Carey, E.V.: Comparing net ecosystem exchange of carbon dioxide between an old-growth and mature forest in the Upper Midwest, USA, Agric. Forest Met., 128, 33-55, 2005.

Desai, A.R., Xu, K., Tian, H., Weishampel, P., Thom, J., Baumann, D., Andrews, A.E., Cook, B.D., King, J.Y., and Kolka, R.: Landscape-level terrestrial methane flux observed from a very tall tower, Agric. Forest Met., 201, 61-75, 2015.

Dunn, A.L., Barford, C.C., Wofsy, S.C., Goulden, M.L., and Daube, B.C.: A long-term record of carbon exchange in a boreal black spruce forest: Means, responses to interannual variability, and decadal trends, Glob. Change Biol., 13, 577-590, 2007.

Fares, S., Savi, F., Muller, J., Matteucci, G., and Paoletti, E.: Simultaneous measurements of above and below canopy ozone fluxes help partitioning ozone deposition between its various sinks in a Mediterranean Oak Forest, Agric. For. Meteorol., 198–199, 181–191, 2014.

Fischer, M.L., Torn, M.S., Billesbach, D.P., Doyle, G., Northup, B., and Biraud, S.C.: Carbon, water, and heat flux responses to experimental burning and drought in a tallgrass prairie, Agric. For. Meteorol., 166-167, 169-174, 2012.

Galvagno, M., Wohlfahrt, G., Cremonese, E., Rossini, M., Colombo, R., Filippa, G., Julitta, T., Manca, G., Siniscalco, C., di Cella, U.M., and Migliavacca, M.: Phenology and carbon dioxide source/sink strength of a subalpine grassland in response to an exceptionally short snow season, Environ. Res. Lett., 8, 025008, 2013.

Hinko-Najera, N., Isaac, P., Beringer, J., van Gorsel, E., Ewenz, C., McHugh, I., Exbrayat, J.-F., Livesley, S. J., and Arndt, S. K.: Net ecosystem carbon exchange of a dry temperate eucalypt forest, Biogeosci., 14, 3781–3800, https://doi.org/10.5194/bg-14-3781-2017, 2017.

Hutley, L. B., Beringer, J., Isaac, P.R., Hacker, J.M., and Cernusak, L.A.: A sub-continental scale living laboratory: Spatial patterns of savanna vegetation over a rainfall gradient in northern Australia, Agric. For. Meteorol., 151, 1417–1428, 2011.

Imer, D., Merbold, L., Eugster, W., and Buchmann, N.: Temporal and spatial variations of soil CO_2, CH_4 and N_2O fluxes at three differently managed grasslands, Biogeosci., 10, 5931–5945, 2013.

Jacobs, C.M.J., Jacobs, A.F.G., Bosveld, F.C., Hendriks, D.M.D., Hensen, A., Kroon, P.S., Moors, E.J., Nol, L., Schrier-Uijl, A., and Veenendaal, E.M.: Variability of annual CO_2 exchange from Dutch grasslands, Biogeosci., 4, 803–816, 2007.

Kato, T., Tang, Y., Gu, S., Hirota, M., Du, M., Li, Y., and Zhao, X.: Temperature and biomass influences on interannual changes in CO2 exchange in an alpine meadow on the Qinghai-Tibetan Plateau, Glob. Chang. Biol., 12, 1285–1298, 2006.

Kilinc, M., Beringer, J., Hutley, L.B., Tapper, N.J., and McGuire, D. A.: Carbon and water exchange of the world's tallest angiosperm forest, Agric. For. Meteorol., 182–183, 215–224, 2013.

Kurbatova, J., Li, C., Varlagin, A., Xiao, X., and Vygodskaya, N.: Modeling carbon dynamics in two adjacent spruce forests with different soil conditions in Russia, Biogeosci., 5, 969–980, 2008.

Leuning, R., Cleugh, H.A., Zegelin, S.J., and Hughes, D.: Carbon and water fluxes over a temperate *Eucalyptus* forest and a tropical wet/dry savanna in Australia: measurements and comparison with MODIS remote sensing estimates, Agric. For. Meteorol., 129, 151–173, 2005.

Ma, S., Baldocchi, D.D., Xu, L., and Hehn, T.: Inter-annual variability in carbon dioxide exchange of an oak/grass savanna and open grassland in California, Agric. For. Meteorol., 147, 157-171, 2007

Marchesini, L.B., Papale, D., Reichstein, M., Vuichard, N., Tchebakova, N., and Valentini, R.: Carbon balance assessment of a natural steppe of southern Siberia by multiple constraint approach, Biogeosci., 4, 581-595, 2007.

Marcolla, B., Cescatti, A., Manca, G., Zorer, R., Cavagna, M., Fiora, A., Gianelle, D., Rodeghiero, M., Sottocornola, M., and Zampedri, R.: Climatic controls and ecosystem responses drive the inter-annual variability of the net ecosystem exchange of an alpine meadow, Agric. For. Meteorol., 151, 1233–1243, 2011.

McHugh, I.D., Beringer, J., Cunningham, S.C., Baker, P.J., Cavagnaro, T.R., MacNally, R., and Thompson, R. M.: Interactions between nocturnal turbulent flux, storage and advection at an “ideal” eucalypt woodland site, Biogeosci., 14, 3027-3050, 2017.

Merbold, L., Ardö, J., Arneth, A., Scholes, R.J., Nouvellon, Y., de Grandcourt, A., Archibald, S., Bonnefond, J.M., Boulain, N., Brueggemann, N., Bruemmer, C., Cappelaere, B., Ceschia, E., El-Khidir, H.A.M., El-Tahir, B.A., Falk, U., Lloyd, J., Kergoat, L., Dantec, V.L., Mougin, E., Muchinda, M., Mukelabai, M.M., Ramier, D., Roupsard, O., Timouk, F., Veenendaal, E.M., and Kutsch, W. L.: Precipitation as driver of carbon fluxes in 11 African ecosystems, Biogeosci., 6, 1027–1041, 2009.

Meyer, W. S., Kondrlovà, E., and Koerber, G.R.: Evaporation of perennial semi-arid woodland in southeastern Australia is adapted for irregular but common dry periods, Hydrol. Process., 29, 3714–3726, 2015.

Noormets, A., Chen, J., and Crow, T.R.: Age-dependent changes in ecosystem carbon fluxes in managed forests in northern Wisconsin, USA, Ecosystems, 10, 187-203, 2007.

Papale, D., Migliavacca, M., Cremonese E., Cescatti, A., et al.: Carbon, Water and Energy Fluxes of Terrestrial Ecosystems in Italy, in "The Greenhouse Gas Balance of Italy" edited by R. Valentini and F. Miglietta, Springer-Verlag Berlin Heidelberg, doi: 10.1007/978-3-642-32424-6_2, 2015

Posse, G., Lewczuk, N., Richter, K., and Cristiano, P.: Carbon and water vapor balance in a subtropical pine plantation, iForest, 9, 736–742, 2016.

Post, H., Hendricks Franssen, H.J., Graf, A., Schmidt, M., and Vereecken, H.: Uncertainty analysis of eddy covariance CO_2 flux measurements for different EC tower distances using an extended two-tower approach, Biogeosci., 12, 1205–1221, 2015.

Powell, T.L., Bracho, R., Li, J., Dore, S., Hinkle, C.R., and Drake, B.G.: Environmental controls over net ecosystem carbon exchange of scrub oak in central Florida, Agric. Forest Meteorol., 141, 19-34, https://doi.org/10.1016/j.agrformet.2006.09.002, 2006.

Prescher, A.-K., Grünwald, T., and Bernhofer, C: Land use regulates carbon budgets in eastern Germany: From NEE to NBP. Agric. For. Meteorol., 150, 1016-1025, 2010.

Prober, S. M., Thiele, K. R., Rundel, P.W., Yates, C. J., Berry, S. L., Byrne, M., Christidis, L., Gosper, C. R., Grierson, P. F., Lemson, K., Lyons, T., Macfarlane, C., O’Connor, M. H., Scott, J. K., Standish, R. J., Stock, W. D., van Etten, E. J., Wardell-Johnson, G. W., and Watson, A.: Facilitating adaptation of biodiversity to climate change: A conceptual framework applied to the world’s largest Mediterranean-climate woodland, Clim. Change, 110, 227–248, https://doi.org/10.1007/s10584-011-0092-y, 2012.

Rambal, S., Joffre, R., Ourcival, J.M., Cavender-Bares, J., and Rocheteau, A.: The growth respiration component in eddy CO_2 flux from a *Quercus ilex* mediterranean forest, Glob. Chang. Biol., 10, 1460–1469, 2004.

Reverter, B.R., Sánchez-Cañete, E.P., Resco, V., Serrano-Ortiz, P., Oyonarte, C., and Kowalski, A.S.: Analyzing the major drivers of NEE in a Mediterranean alpine shrubland, Biogeosci., 7, 2601–2611, 2010.

Schroder, I., Kuske, T., and Zegelin, S.: Eddy covariance dataset for Arcturus (2011-2013), Geoscience Australia, Canberra, doi:102.100.100/14249, 2014.

Scott, R.L., Biederman, J.A., Hamerlynck, E.P., and Barron-Gafford, G.A.: The carbon balance pivot point of southwestern U.S. semiarid ecosystems: Insights from the 21st century drought, J. Geophys. Res. Biogeosci., 120, 2612-2624, 2015a.

Scott, R.L., Hamerlynck, E.P., Jenerette, G.D., Moran, M.S., and Barron-Gafford, G.: Carbon dioxide exchange in a semidesert grassland through drought-induced vegetation change, J. Geophys. Res. Biogeosci., 115, G03026, doi:10.1029/2010JG001348, 2010.
Scott, R.L., Jenerette, G.D., Potts, D.L., and Huxman, T.E.: Effects of seasonal drought on net carbon dioxide exchange from a woody-plant-encroached semiarid grassland, J. Geophys. Res. Biogeosci., 114, G04004, doi:10.1029/2008JG000900, 2009.
Serrano-Ortiz, P., Marañón-Jiménez, S., Reverter, B.R., Sánchez-Cañete, E.P., Castro, J., Zamora, R., and Kowalski, A.S.: Post-fire salvage logging reduces carbon sequestration in Mediterranean coniferous forest, Forest Ecol. Man., 262, 2287-2296, https://doi.org/10.1016/j.foreco.2011.08.023, 2011
Stevens, R.M., Ewenz, C.M., Grigson, G., and Conner, S.M.: Water use by an irrigated almond orchard, Irrig. Sci., 30, 189–200, 2012.
Suni, T., Rinne, J., Reissell, A., Altimir, N., Keronen, P., Rannik, Ü., Maso, M.D., Kulmala, M., and Vesala, T.: Long-term measurements of surface fluxes above a Scots pine forest in Hyytiälä, southern Finland, 1996–2001, Boreal Environ. Res., 8, 287–301, 2003.
Ulke, A.G., Gattinoni, N.N., and Posse, G.: Analysis and modelling of turbulent fluxes in two different ecosystems in Argentina, Int. J. Environ. Pollut., 58, 52–62, 2015.
Valentini, R., De Angelis, P., Matteucci, G., Monaco, R., Dore, S., and Mugnozza, G. E. S.: Seasonal net carbon dioxide exchange of a beech forest with the atmosphere, Glob. Chang. Biol., 2, 199–207, 1996.
Wick, B., Veldkamp, E., De Mello, W.Z., Keller, M., and Crill, P.: Nitrous oxide fluxes and nitrogen cycling along a pasture chronosequence in central Amazonia, Brazil, Biogeosci., 2, 175-187, 2005.
Yee, M.S., Pauwels, V.R.N., Daly, E., Beringer, J., Rüdiger, C., McCabe, M.F., and Walker, J.P.: A comparison of optical and microwave scintillometers with eddy covariance derived surface heat fluxes, Agric. For. Meteorol., 213, 226–239, 2015.

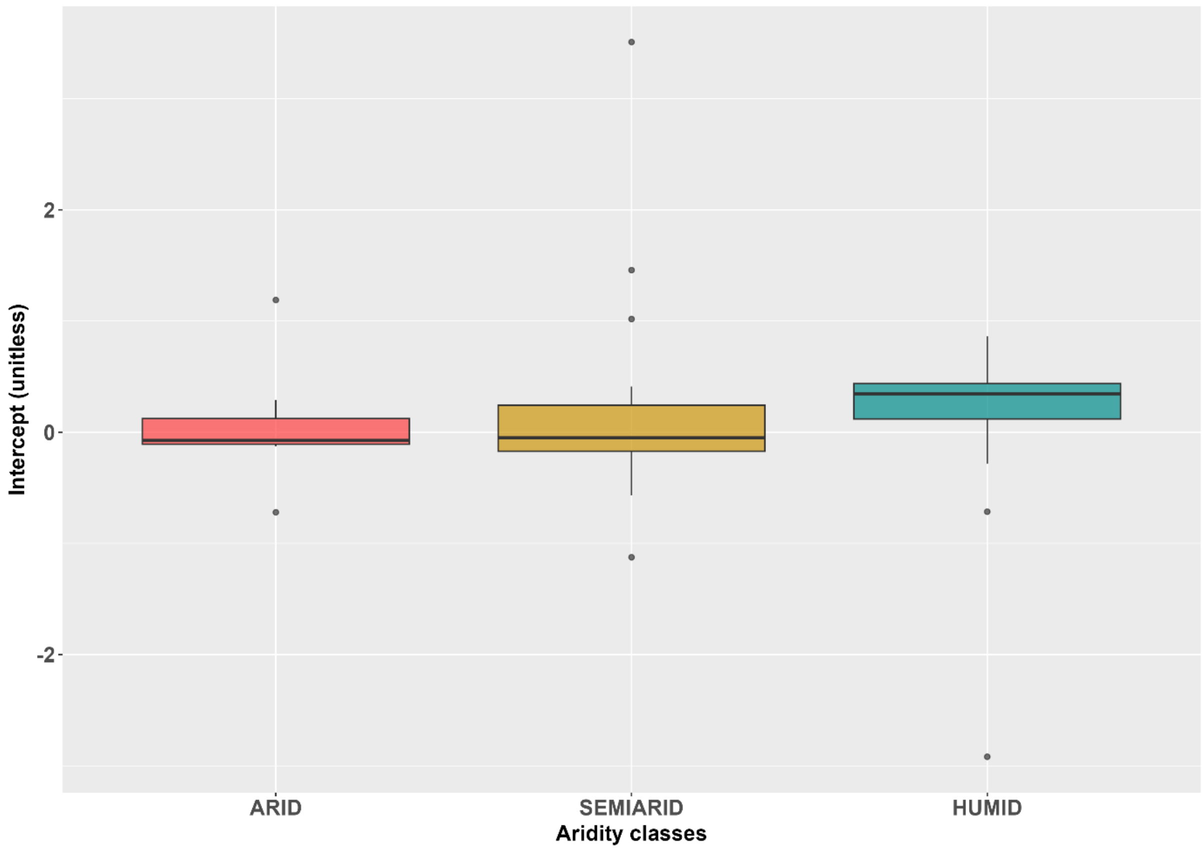

Supplementary Figure 1: Box-plot showing the range of intercept values obtained across all the flux tower sites, grouped by aridity class. The black line is the median value, the box is the interquartile range and the whiskers show the range, with outliers shown as asterisks. The median value is not significantly different from zero.

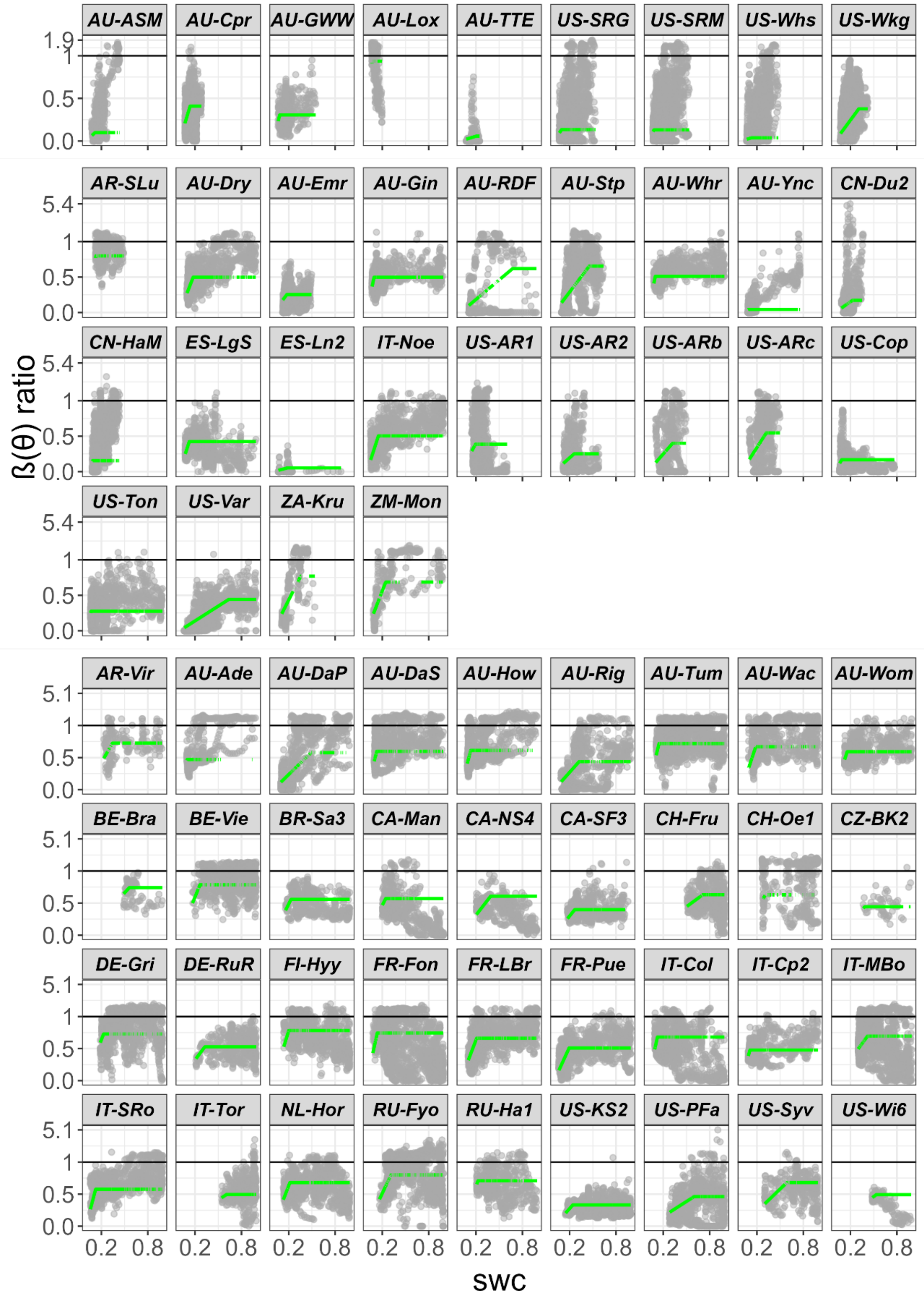

Supplementary Figure 2: Values of the fitted maximum β(θ) ratio (the ratio of actual flux-derived to modelled well-watered gross primary production) and the critical threshold value of soil moisture for all 67 sites used in the analysis, where the intercept is assumed to be zero. The βθ ratio and the soil water content (swc) are both unitless. Note that the scale above 1 has been compressed for visualization purposes.

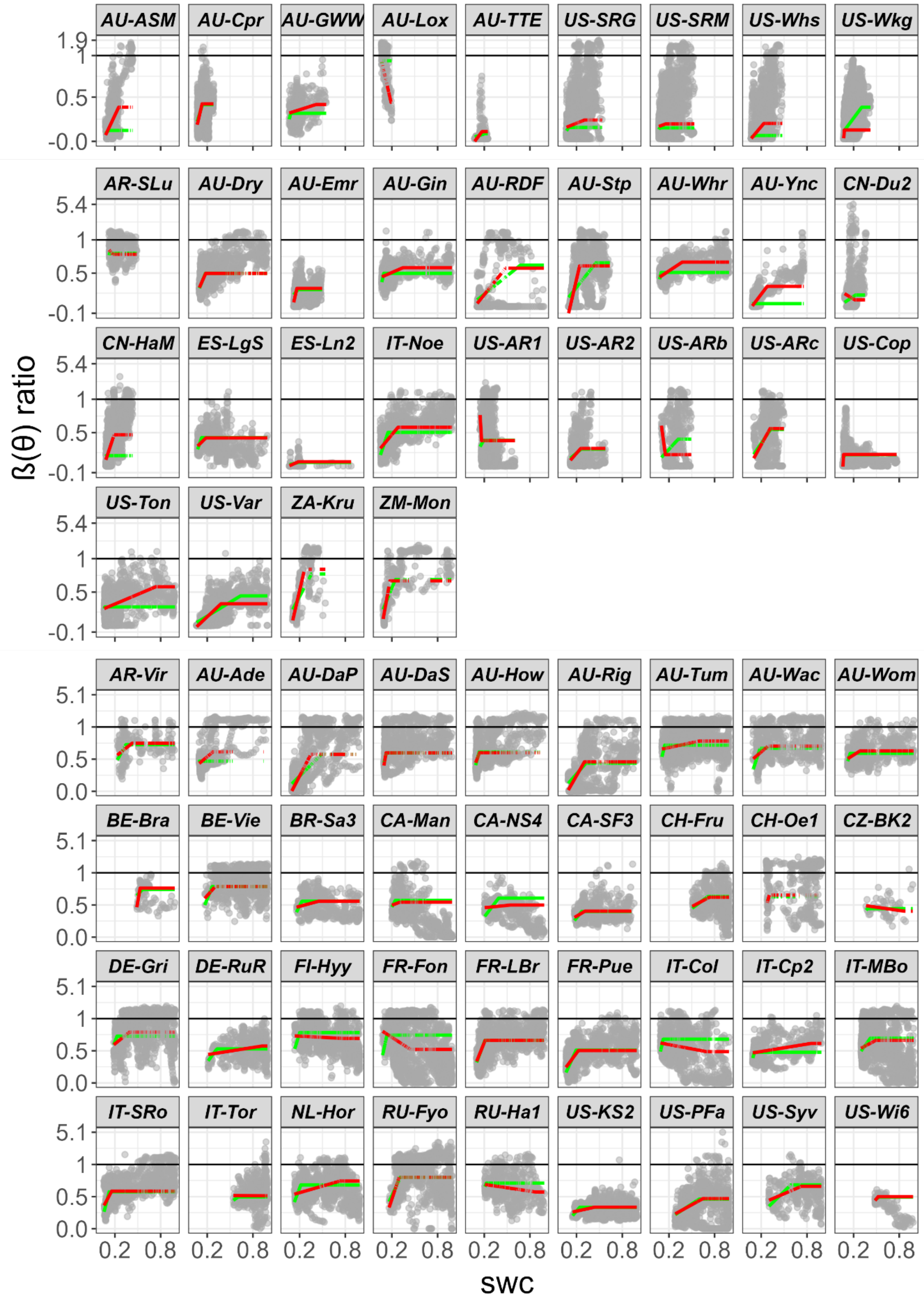

Supplementary Figure 3: Values of the fitted maximum β(θ) ratio (the ratio of actual flux-derived to modelled well-watered gross primary production) and the critical threshold value of soil moisture for all 67 sites used in the analysis, where the intercept is assumed to be zero (green line) or not fixed (red line). The βθ ratio and the soil water content (swc) are both unitless. Note that the scale above 1 has been compressed for visualization purposes.

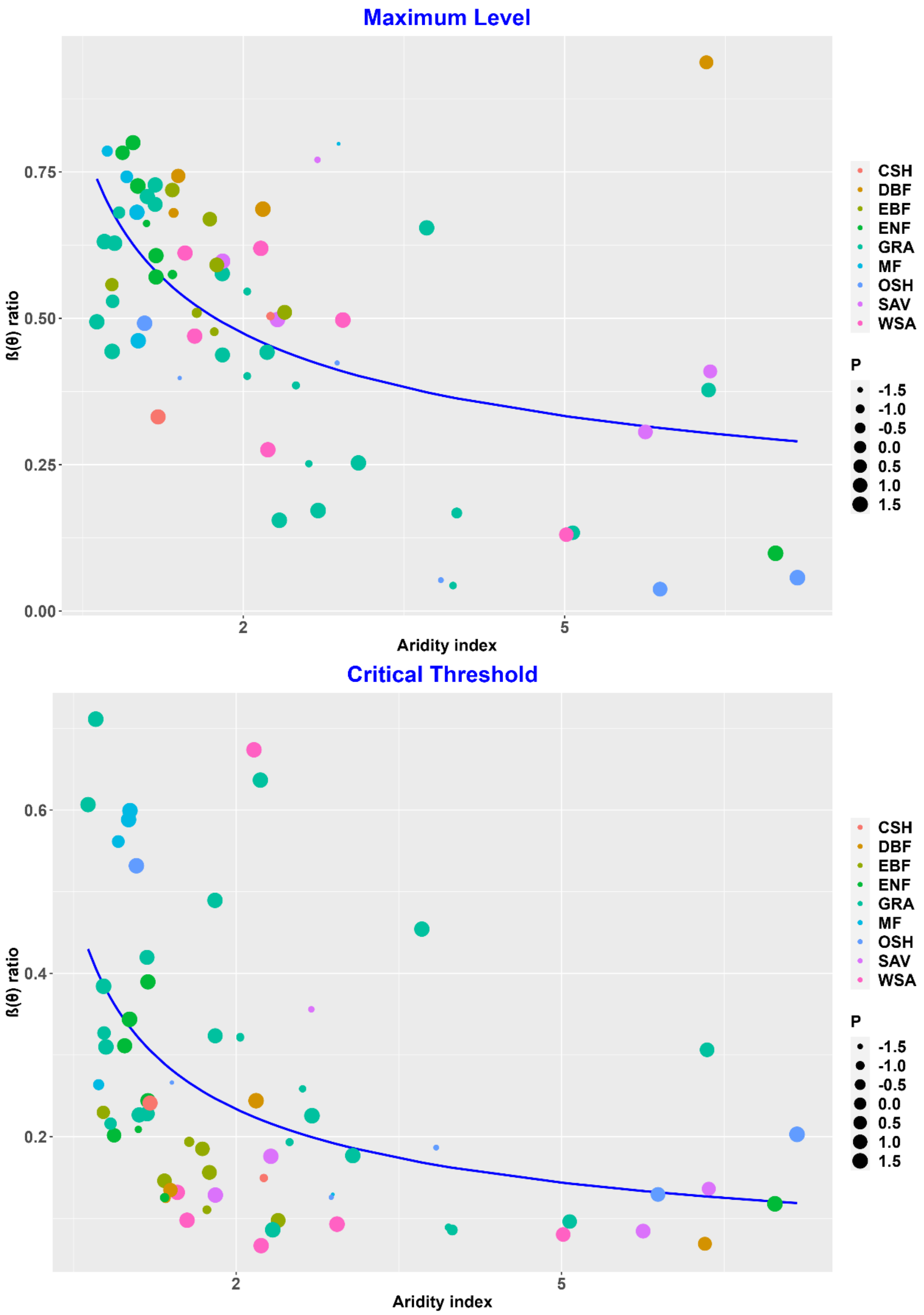

Supplementary Figure 4: The fitted non-linear regression model of the maximum level (top) and the critical threshold (bottom) of the β(θ) ratio (the ratio of observed to predicted gross primary production) against the aridity index, where the sites are classified according to vegetation type and precipitation phase.

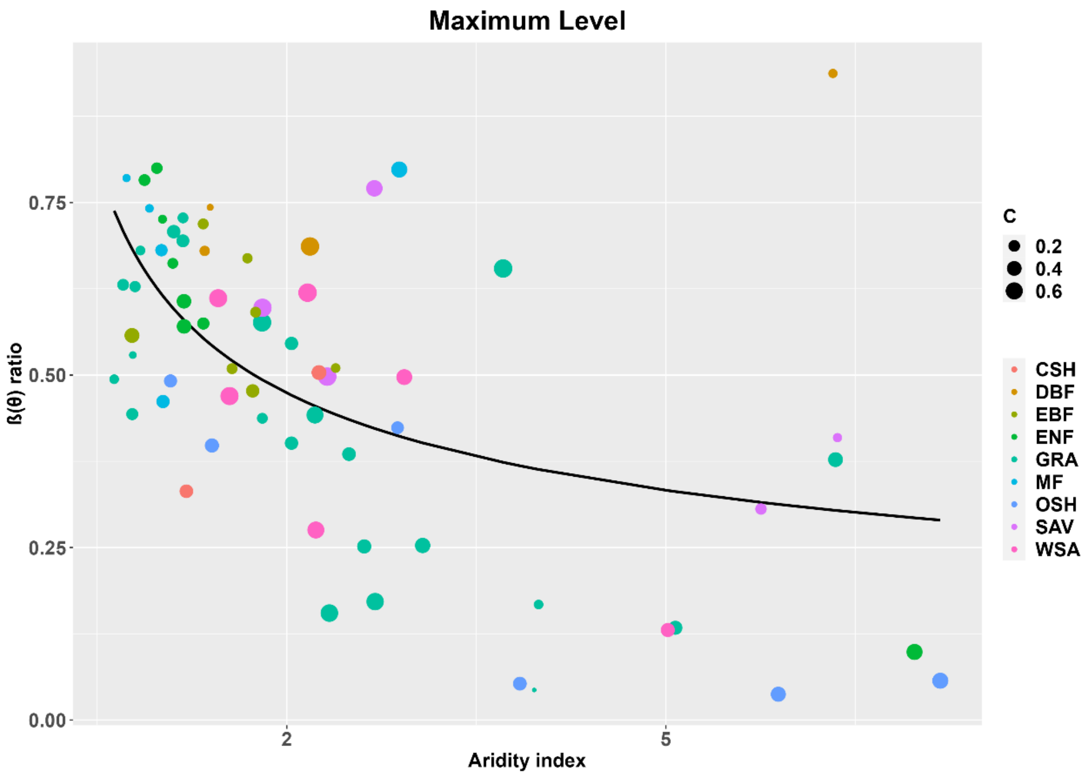

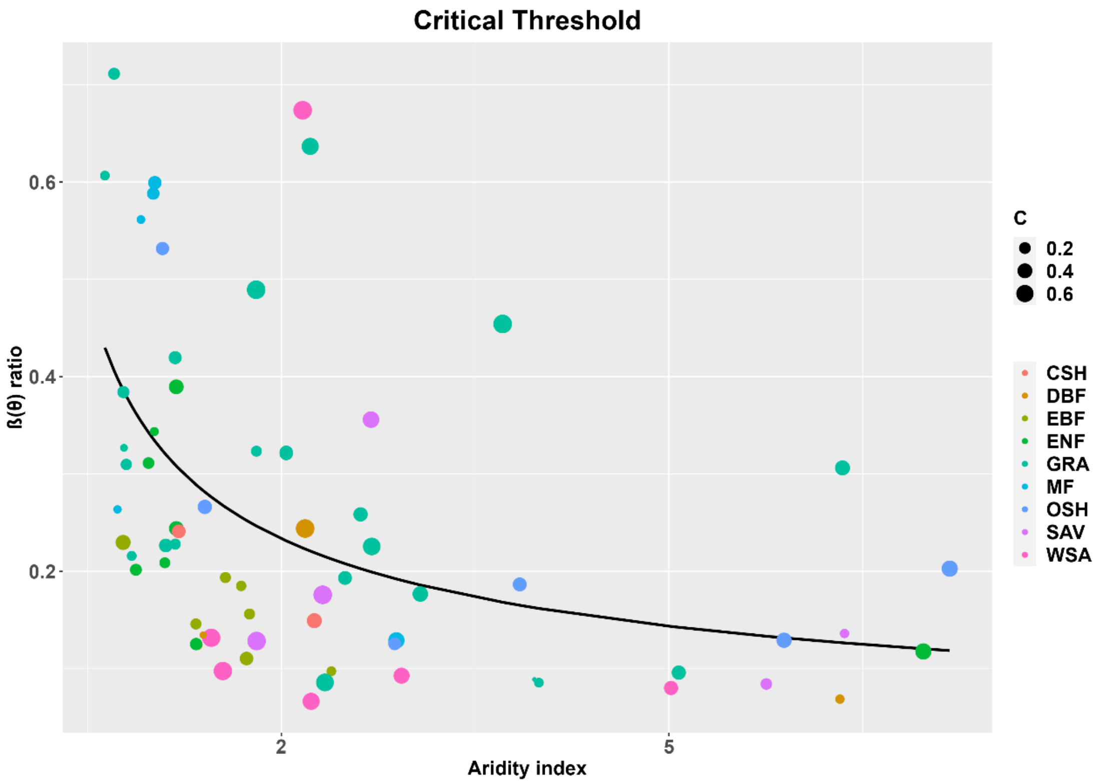

Supplementary Figure 5: The fitted non-linear regression model of the maximum level (top) and the critical threshold (bottom) of the β(θ) ratio (the ratio of observed to predicted gross primary production) against the aridity index, where the sites are classified according to according to vegetation type and precipitation concentration.

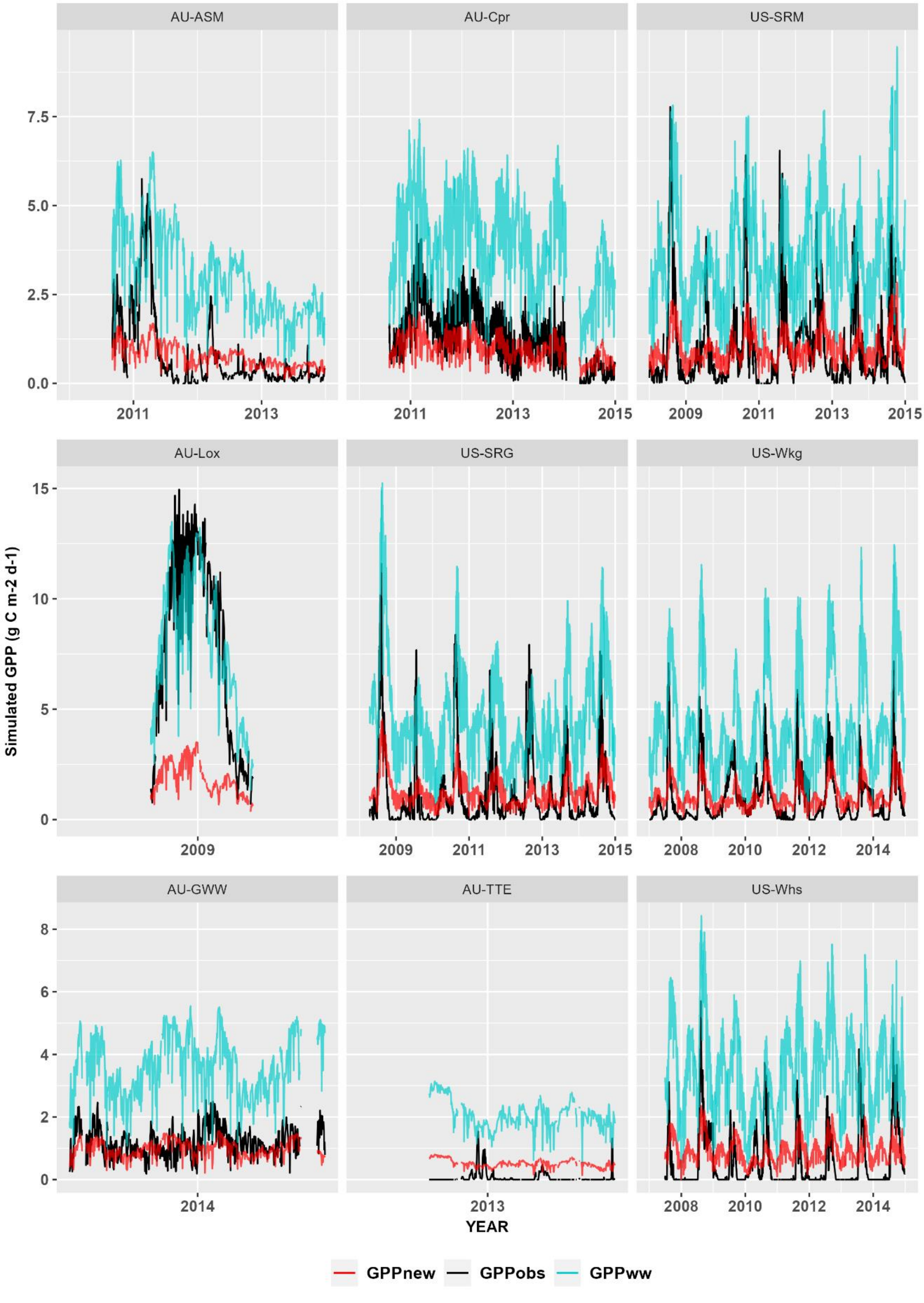

Supplementary Figure 6: The impact of the application of the new soil moisture stress function on simulated gross primary production (GPP_{new}) at flux tower sites classified as arid (aridity index, AI >5). The new model is compared to the simulated level of GPP under well-watered conditions (GPP_{ww}) and to flux-derived values (GPP_{obs}).

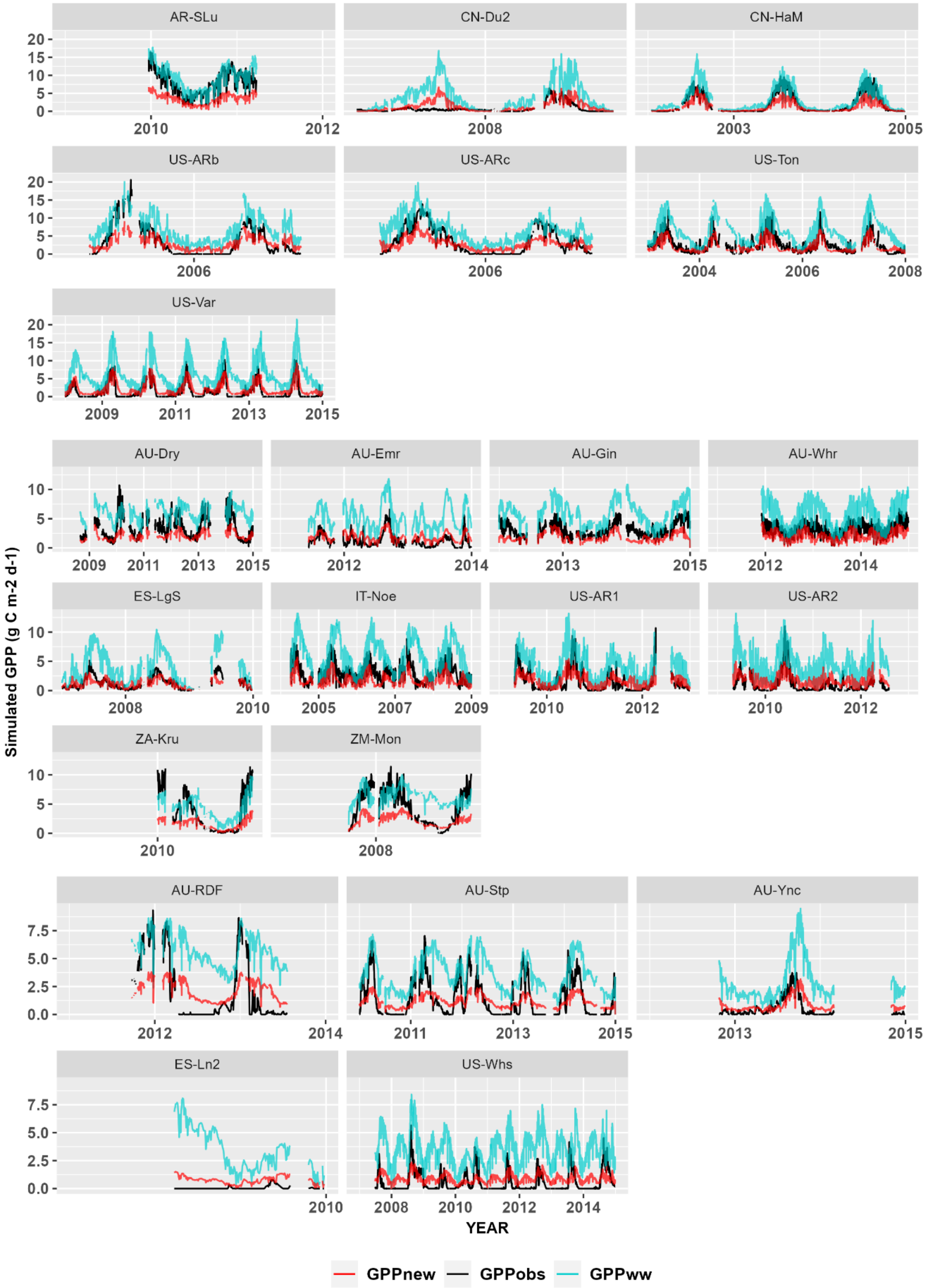

Supplementary Figure 7: The impact of the application of the new soil moisture stress function on simulated gross primary production (GPP_{new}) at flux tower sites classified as semi-arid (aridity index, AI between 2 and 5). The new model is compared to the simulated level of GPP under well-watered conditions (GPP_{ww}) and to flux-derived values (GPP_{obs}).

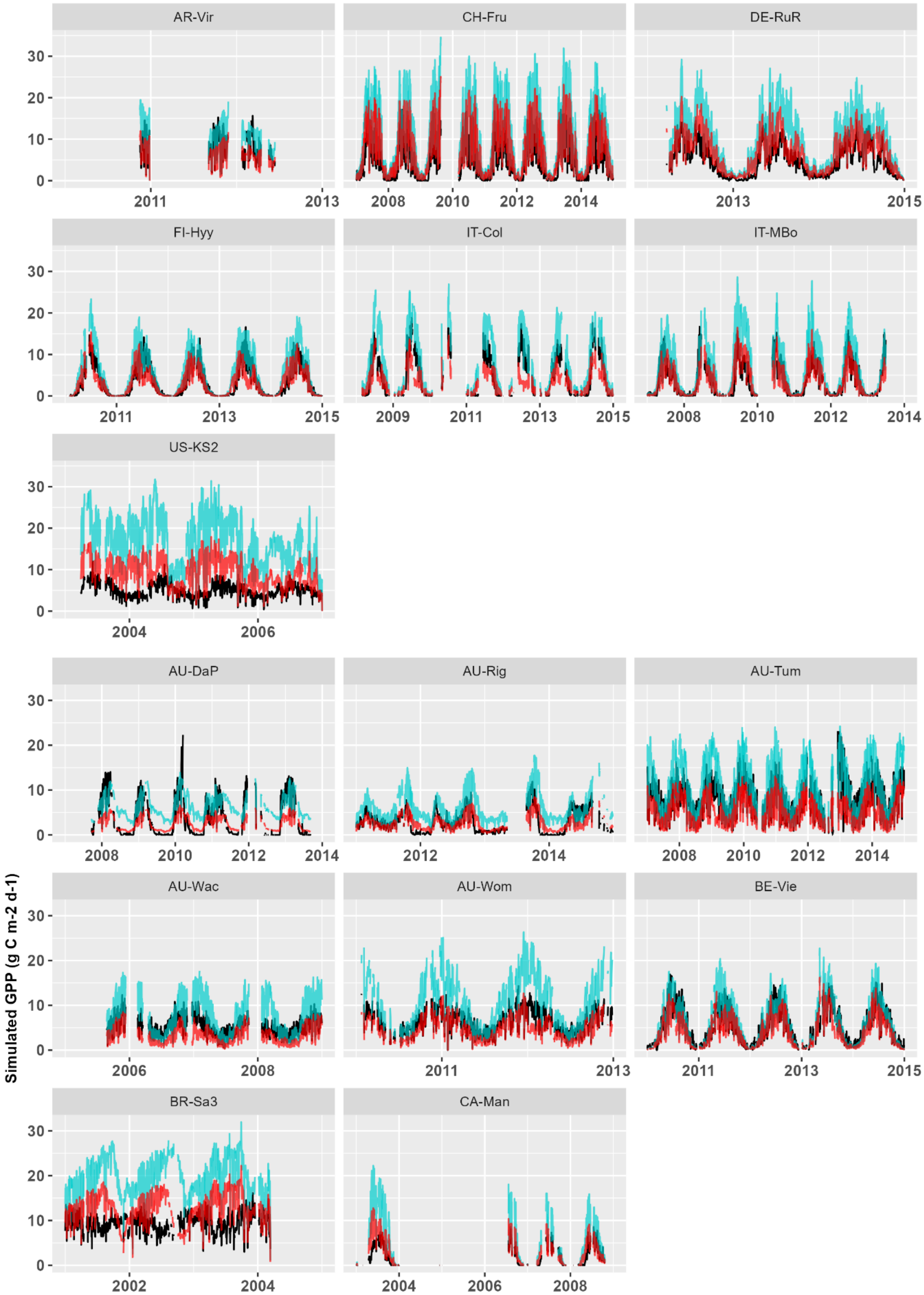

Supplementary Figure 8: The impact of the application of the new soil moisture stress function on simulated gross primary production (GPP_{new}) at flux tower sites classified as humid (aridity index, AI <2). The new model is compared to the simulated level of GPP under well-watered conditions (GPP_{ww}) and to flux-derived values (GPP_{obs}).

Figure 8 (continued)

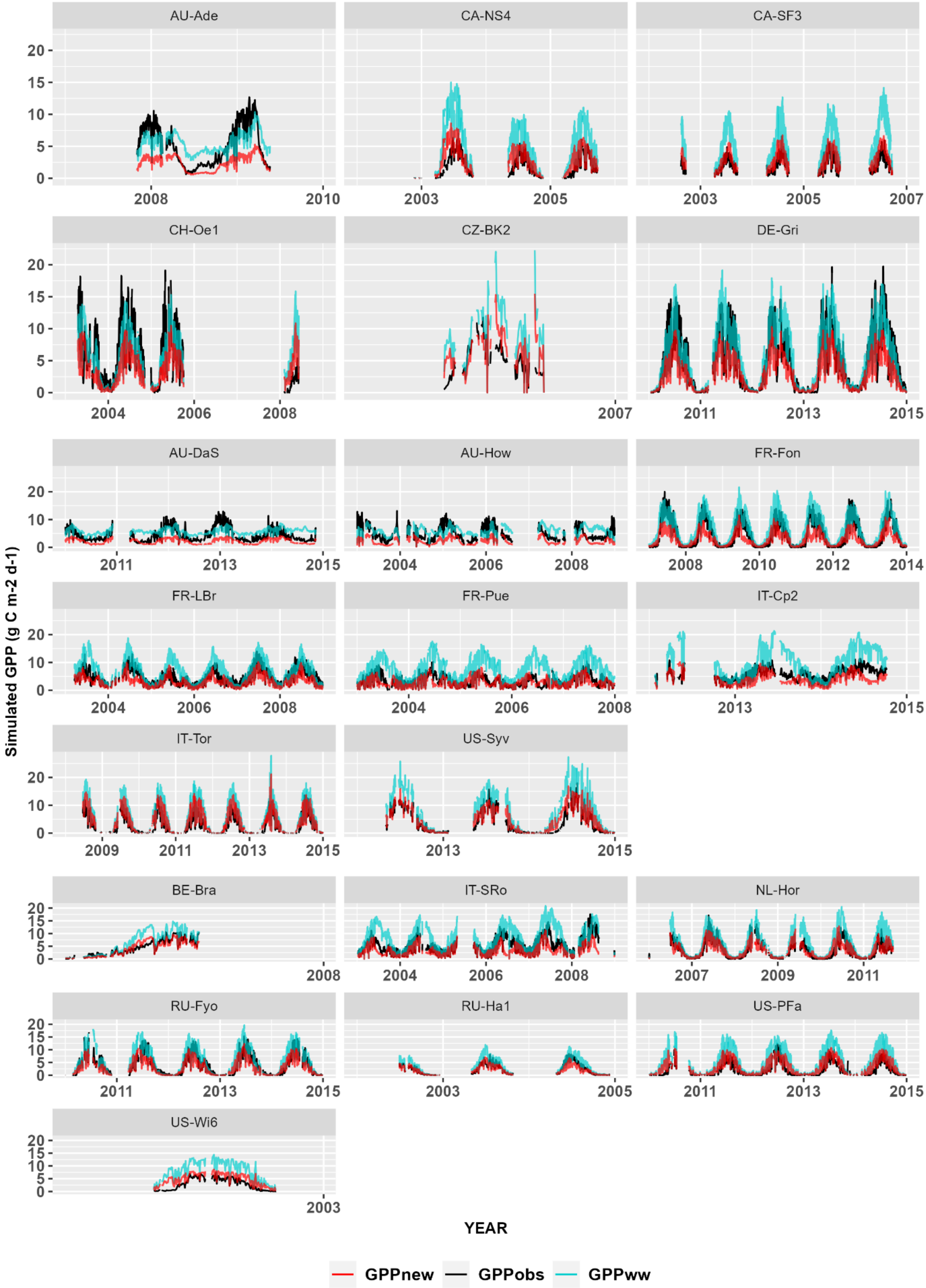

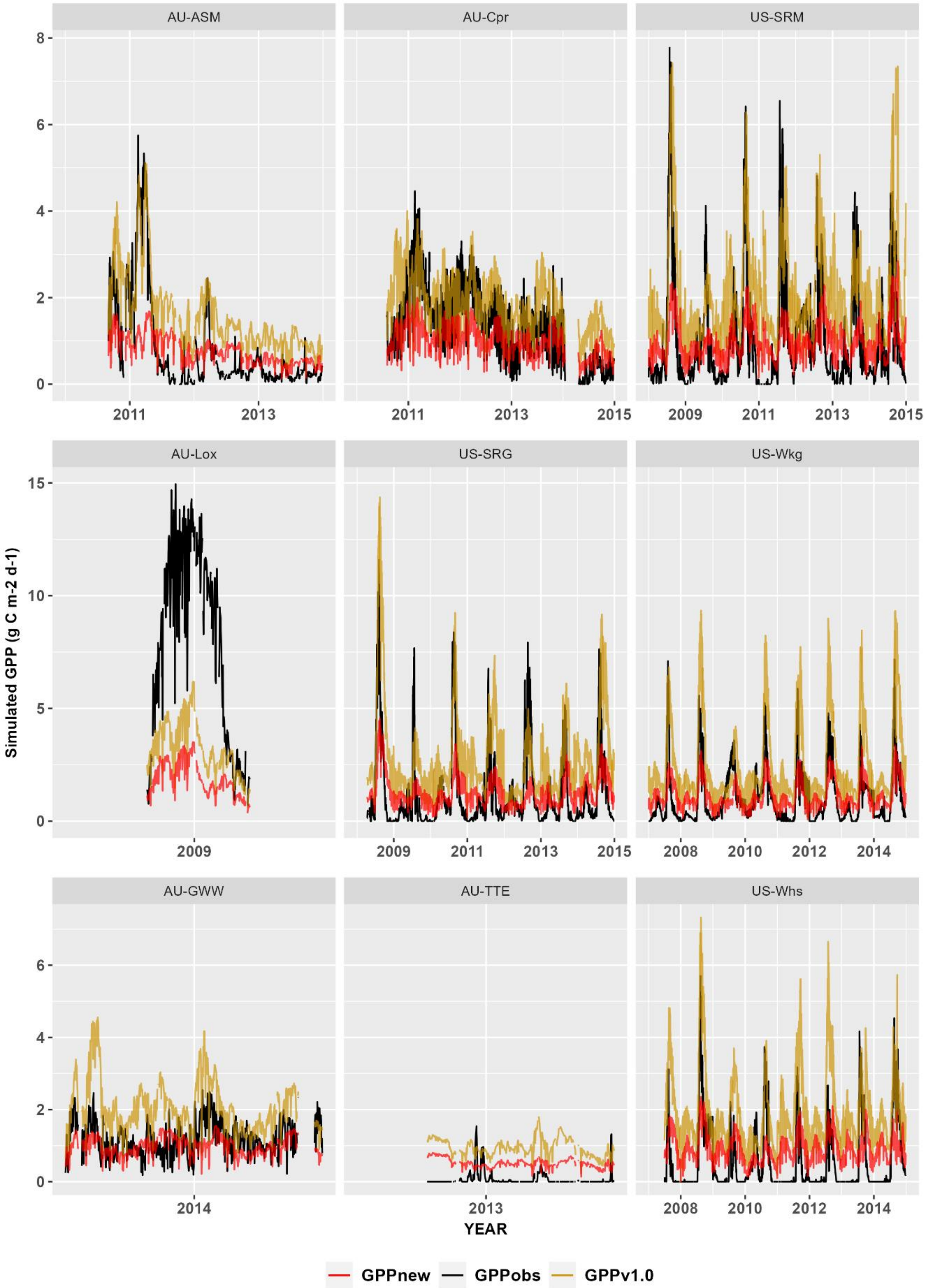

Supplementary Figure 9: Comparison of simulated gross primary production including the new soil-moisture stress function (GPP_{new}) and the original stress function ($GPP_{v1.0}$) from Stocker et al. (2020) against flux-derived values (GPP_{obs}) at flux tower sites classified as arid (aridity index, AI > 5).

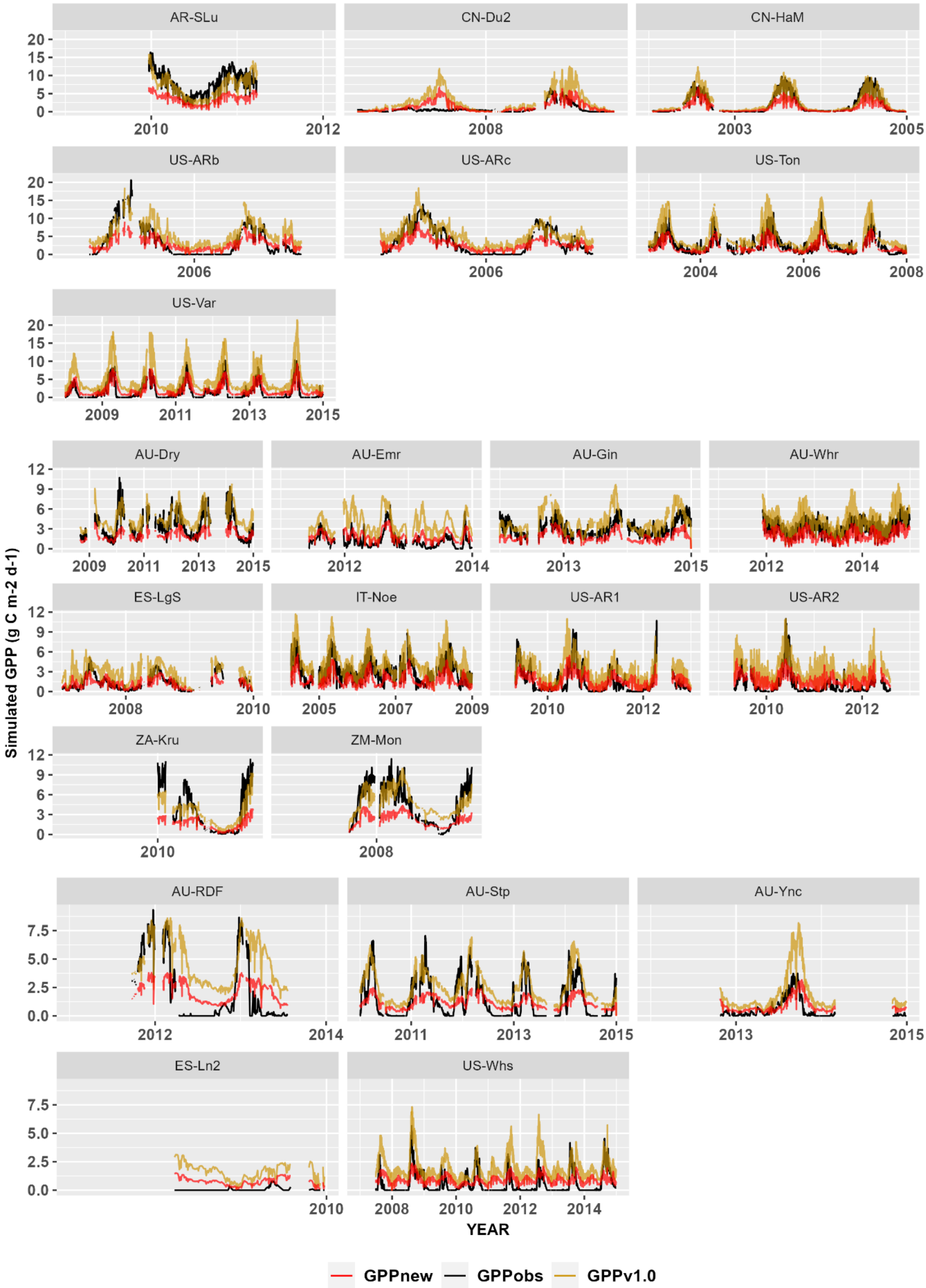

Supplementary Figure 10: Comparison of simulated gross primary production including the new soil-moisture stress function (GPP_{new}) and the original stress function ($GPP_{v1.0}$) from Stocker et al. (2020) against flux-derived values (GPP_{obs}) at flux tower sites classified as semi-arid (aridity index, AI = between 2 and 5).

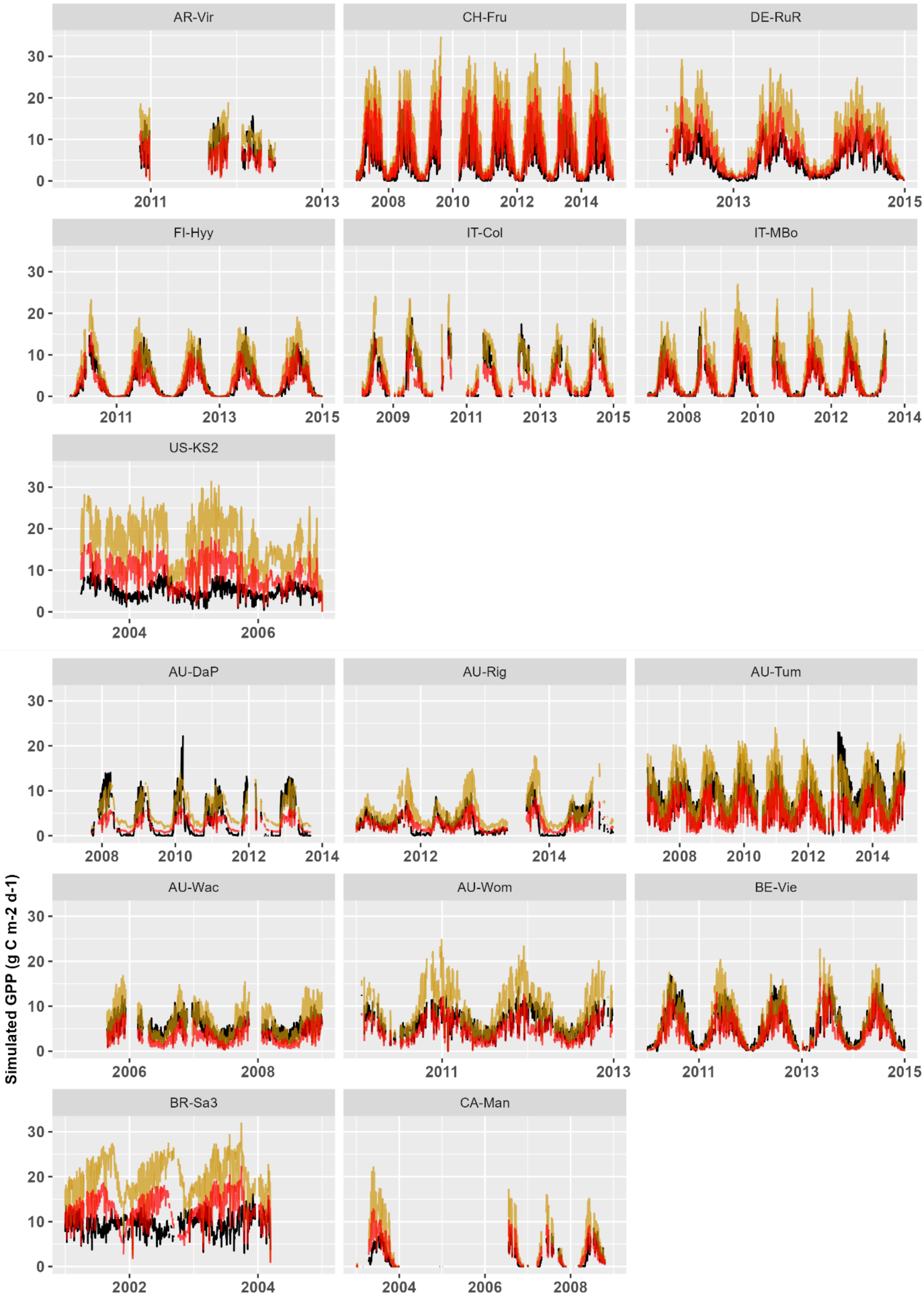

Supplementary Figure 11: Comparison of simulated gross primary production including the new soil-moisture stress function (GPP_{new}) and the original stress function ($GPP_{v1.0}$) from Stocker et al. (2020) against flux-derived values (GPP_{obs}) at flux tower sites classified as humid (aridity index, AI < 2).

Figure 11 (continued)